Advanced Synthesis & Catalysis

DOI: 10.1002/adsc.201500039

Design of Nitrilases with Superior Activity and Enantioselectivity towards Sterically Hindered Nitrile by Protein Engineering

Ya-Ping Xue,[a,b] Cheng-Ci Shi,[a,b] Zhe Xu,[a,b] Biao Jiao,[a,b] Zhi-Qiang Liu,[a,b] Jian-Feng Huang,[a,b] Yu-Guo Zheng,[a,b,*] and Yin-Chu Shen[a,b]

[a] Institute of Bioengineering, Zhejiang University of Technology, Hangzhou 310014, People's Republic of China
Fax: (+86)-571-8832-0630; phone: (+86)-571-8832-0630; e-mail: zhengyg@zjut.edu.cn
[b] Engineering Research Center of Bioconversion and Biopurification of Ministry of Education, Zhejiang University of Technology, Hangzhou 310014, People's Republic of China

Received: January 25, 2015; Revised: March 16, 2015; Published online: ■■ ■■, 0000

Supporting information for this article is available on the WWW under http://dx.doi.org/10.1002/adsc.201500039.

Abstract: The enantioselective hydrolysis of *ortho*-chloromandelonitrile with nitrilase is one of the most attractive approaches to prepare (*R*)-*ortho*-chloromandelic acid. To date, efforts to develop this nitrilase-mediated process were plagued by either insufficient ee_p (enantiomeric excess of product) or low activity due to the steric hindrance from the *ortho*-substituted substrate. To improve the nitrilase potential for producing (*R*)-*ortho*-chloromandelic acid, an enhancement of both activity and enantioselectivity towards sterically hindered nitriles would be highly desirable. Molecular docking of the (*R*)-*ortho*-chloromandelonitrile into the active site of wild-type 2A6 nitrilase (nitA) allowed the identification of proximal nitA active site residues. Several residues (52, 132, 189 and 190) were selected as targets for single and double point mutation to improve nitA activity and enantioselectivity towards *ortho*-chloromandelonitrile. Targeted mutagenesis yielded several nitA variants with superior activity and enantioselectivity. The best mutant T132A/F189T exhibited a 4.37-fold higher specific activity (7.39 U/mg) towards *ortho*-chloromandelonitrile than the wild-type nitA. More importantly, the enantioselectivity (E) was improved from 17.34 to >200, resulting in a highly enantiopure product. Molecular docking experiments further support the enhanced activity and enantioselectivity shown experimentally and the structural effects of this amino acid substitution on the active site of nitA are provided. The amino acids at sites 189 and 132 determine the activity and enantioselectivity towards *ortho*-chloromandelonitrile. With mutant T132A/F189T as a catalyst, a maximum of 450 mM of (*R*)-*ortho*-chloromandelic acid was produced with a 90% conversion and >99% ee_p within 3 h. This is the first time that a high productivity of (*R*)-*ortho*-chloromandelic acid of up to 671.76 $g\,L^{-1}\,d^{-1}$ using a nitrilase-mediated approach is reported. The engineered T132A/F189T variant represents a promising and competitive biocatalyst for practical application in synthesizing (*R*)-*ortho*-chloromandelic acid.

Keywords: biocatalysis; enantioselectivity; kinetic resolution; mutagenesis; nitrilase; protein engineering

Introduction

Enantiomerically pure 2-hydroxyarylacetic acids are valuable intermediates and building blocks for the synthesis of biologically active compounds and target molecules.[1] For instance, (*R*)-2-chloromandelic acid [(*R*)-**2a**] is emerging as the preferred chiral intermediate for the industrial synthesis of the anti-thrombotic agent (*S*)-clopidogrel.[2] World-wide sales of (*S*)-clopidogrel amount to several billion dollars per year. Presently, resolution is the most popular way to prepare chiral 2-hydroxyarylacetic acids in industry.[3] Resolution procedures include diastereomeric crystallization[4] and enantioselective enzymatic hydrolysis of the *O*-acetates or esters of hydroxy acids.[5] Nevertheless, the yield of such approaches is limited to only 50%. The nitrilase-mediated resolution has exciting potential for synthesizing (*R*)-2-hydroxyarylacetic acids from nitriles due to the cheap starting material and the 100% theoretical yield[6] (Scheme 1). Nitrilases (EC 3.5.5.1) represent a class of hydrolytic enzymes which catalyze the hydrolysis of nitriles to the corresponding carboxylic acids in one single step. The nitrilase-catalyzed processes to produce carboxylic

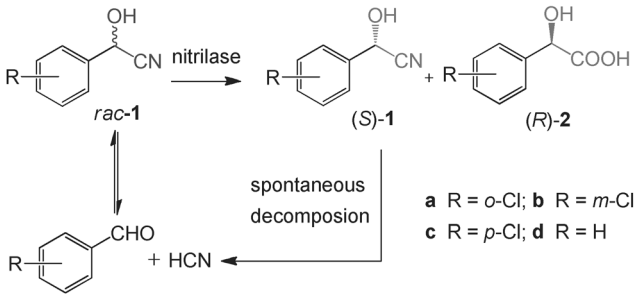

Scheme 1. Enantioselective hydrolysis of *rac*-**1** for the production of (*R*)-**2** with nitrilase. The residual (*S*)-**1** which is unreactive to the nitrilase spontaneously decomposed to aldehyde plus cyanide, which was then converted to substrate for the nitrilase.

acids from nitriles are often preferred to chemical hydrolysis because the reactions do not require strongly acidic or basic reaction conditions and elevated temperatures and produce the desired product with high selectivity at high conversion.[7] Over the past decades, an increasing number of studies on nitrilases has been reported. Nitrilases have been proven to be valuable alternatives to chemical catalysts for the industrial production of fine chemicals such as (*R*)-mandelic acid and pharmaceutical intermediates such as (*R*)-ethyl 3-hydroxyglutarate.[8]

Unfortunately, efforts to develop a nitrilase-mediated hydrolytic process for the economic production of (*R*)-**2a** from racemic *ortho*-chloromandelonitrile (*rac*-**1a**) were plagued by either insufficient ee_p (enantiomeric excess of product) or low activity. All the existing nitrilases performed poorly towards the *ortho*-substituted substrate *rac*-**1a** because of the steric hindrance. Several nitrilases screened from genomic libraries[9] or engineered from *Alcaligenes faecalis*[10] with high enantioselectivity towards *rac*-**1a** were often inhibited by the substrate even at a relatively low concentration (10–20 mM). The nitrilases from *Alcaligenes* sp. ECU0401,[11] *Labrenzia aggregata* DSM 13394[12] and *Burkholderia cenocepacia* J2315[13] could convert a relative high amount of *rac*-**1a** (200–494 mM) with ee_p values of 90.4, 96 and 97.6%, respectively. However, it is still necessary to further improve their enantioselectivity and activity to meet the requirement of industrial applications. In our recent work, more than ten nitrilases were discovered by screening different soil samples[14] and several nitrilase genes from phylogenetically distinct organisms were cloned and expressed.[15] We also engineered the nitrilase from *Alcaligenes faecalis* ZJUTB10[16] to improve its activity towards *rac*-mandelonitrile (*rac*-**1d**). To our disappointment, none of those nitrilases exhibited high enantioselectivity and activity towards *rac*-**1a**. To date, increasing both the enantioselectivity and activity of an enzyme reaction for synthetic advantage represents a difficult problem for the enzyme designers.[17] This is especially the case for the nitrilases towards *rac*-**1a**, where it is difficult to implement a high-throughput method of determining enantioselectivity to allow the rapid screening of a large number of mutants because of racemization of the substrate. The task of searching for novel nitrilases with high activity and excellent enantioselectivity towards sterically hindered nitrile *rac*-**1a** still remains a challenge.[18]

Here, we have designed several nitrilases with superior activity and enantioselectivity towards sterically hindered substrate *rac*-**1a** by protein engineering for the efficient production of (*R*)-**2a** with the preselected 2A6 nitrilase (nitA), which was screened by Robertson et al.[19] The molecular docking experiment of (*R*)-**1a** into the nitA active site was used to identify active site residues that are close to the substrate. The docking experiment identified four positions (52, 132, 189 and 190) in the nitA active site that might be the suitable targets for engineering the acivity and enantioselectivity of nitA towards *rac*-**1a**. These positions were randomized by gene site-saturation mutagenesis (GSSM) and four single-site libraries were created. Three single mutants at positions 132 and 189 with enhanced nitA activity and enantioselectivity towards substrate *rac*-**1a** were obtained. Then, combinatorial saturation mutagenesis libraries at site 132 and 189 were constructed. Several double mutants showed superior activity and excellent enantioselectivity towards substrate *rac*-**1a**, when compared to the wild-type enzyme. A possible mechanism was proposed to explain the experimental observations obtained for the wild-type and mutant nitA. This is the first example of enzyme-substrate docking-guided point mutation of the substrate-binding residues to generate mutant nitrilases with enhanced both activity and enantioselectivity towards *rac*-**1a**. These results provide some insight into the fundamental question of how substrate-binding residues affect substrate binding orientation and thus control the reaction stereoselectivity.

Results and Discussion

Planning of Nitrilase Mutagenesis

The crystal structures of several nitrilase superfamily members were well documented and the first crystal structure of *Pyrococcus abyssi* nitrilase exhibiting true nitrilase activity was recently reported.[20] With the increased number of the enzyme structures available from the Protein Data Bank (PDB) and highly developed bioinformatic tools, design of the "hot spots" which potentially affect the enzymatic activity might significantly increase the efficiency of desired mutant

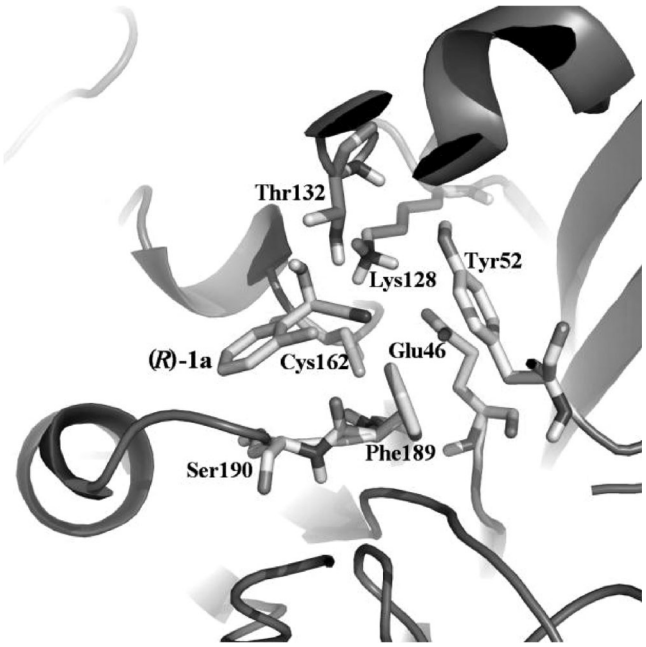

Figure 1. Close-up view of the catalytic residues Glu46-Lys128-Cys162 (medium grey sticks) and mutated active site surrounding residues (Tyr52, Thr132, Phe189 and Ser190) of wild-type (light grey sticks) in complex with the most favorable docked pose for (*R*)-**1a** (dark grey sticks). Docking of substrate was performed using the available tools in AutoDock 4.0.

hits.[21] Based on previous work,[11–13,19] a semi-rational design was chosen to engineer nitA to identify hot spots for subsequent mutations to increase the activity and enantioselectivity. Homology modeling and docking experiments were first performed to gain insights into the binding mode of the (*R*)-**1a** with the active sites of the reported arylacetonitrilases (*Burkholderia cenocepacia* J2315 nitrilase, *Labrenzia aggregate* DSMZ 13394 nitrilase, *Alcaligenes* sp. ECU0401 nitrilase, *A. faecalis* ZJUTB10 nitrilase and nitA). Through a BLAST search against the PDB, the protein PH0642 from *Pyrococcus horikoshii* (PDB accession code 1J31) showed the highest sequence identity to the reported arylacetonitrilases. The 3D structural models of these arylacetonitrilases were constructed based on the crystal structures of protein PH0642. The docking experiments showed that nitA was the most suitable candidate for the semi-rational design of nitrilase mutagenesis with higher activity and enantioselectivity towards (*R*)-**2a** according to the proposed nitrilase reaction mechanism[22] and spatial positions of catalytic pocket and substrate (Supporting Information, Figure S1).

The binding mode of the substrate (*R*)-**1a**, catalytic residues and the active site surrounding residues are shown in Figure 1. According to the proposed nitrilase reaction mechanism,[22] Cys162 attacks the cyano group of nitrile as a nucleophile, Glu46 assumes the role of a general base, and Lys128 is involved in stabilization of the formed tetrahedral intermediate structure. The enantioselectivity and activity of nitrilase should have a close relationship with the spatial conformation of catalytic pocket. Several active site residues (Tyr52, Thr132, Phe189, and Ser190) are in close proximity to the substrate (*R*)-**1a** after a detailed examination (Figure 1). Both Ser190 and Phe189 were located at one side of the catalytic tunnel towards the *ortho*-chloro substituent and the α-hydroxy group of the substrate, which might have a considerable effect on the activity and enantioselectivity towards *rac*-**1a** due to the steric hindrance. The same situation was observed at Thr132. In addition, the hydroxy in the Thr132 has a strong hydrogen bond with the α-hydroxy in the substrate, which might have an effect on the enzyme activity. Tyr52 was an important component at the bottom of the catalytic tunnel. So four residues (Tyr52, Thr132, Phe189 and Ser190) were selected for mutagenesis.

Library Construction and Nitrilase Variants Screening

In order to examine the effect of different amino acid side chains at the four selected positions (52, 132, 189 and 190) on nitA activity and enantioselectivity, four single-site libraries were generated by GSSM. The resulting libraries were screened for clones that exhibited higher activity towards *rac*-**1a**. Cells of the mutant nitA clones from each library were first grown in 96-deep-well plates containing three clones of wild-type nitA as control, after which cells were washed, lysed and assayed separately for their ability to hydrolyze *rac*-**1a**. The formed products were analyzed by chiral HPLC. Overall, 11 out of 744 clones (186 clones for each library) from the four libraries were selected because of their apparent higher activity and enantioselectivity towards *rac*-**1a**. The plasmids from the 11 selected clones were isolated, and the gene sequence analysis showed that the clones contained three mutations (T132R, F189T and F189S). These mutants and wild-type nitA were purified to $>90\%$ homogeneity using an Ni-based immobilized metal affinity chromatography procedure. Further evaluation of the activity and enantioselectivity of the purified enzymes was performed. The results are shown in Table 1. The variants T132R (4.35 U/mg) and F189T (5.87 U/mg) were the best variants with highest activity at site 189 and 132. In addition, the enantioselectivities have also been improved greatly. For the second round of GSSM, a combinatorial saturation mutagenesis library at site 132 was constructed by choosing variant F189T as a template. Meanwhile, the combinatorial saturation mutagenesis library at site 189 was constructed

Table 1. Nitrilase mutants with increased specific activity and enantioselectivity after two rounds of GSSM.[a]

Mutants	Specific activity [U/mg]	ee_p[b] [%]
None (wild-type)	1.69 ± 0.02	86.7
First round		
T132R	4.35 ± 0.09	96.0
F189S	3.82 ± 0.13	98.5
F189T	5.87 ± 0.04	> 99
Second round		
T132R/F189C	5.60 ± 0.11	> 99
T132R/F189S	4.63 ± 0.01	> 99
T132R/F189T	6.02 ± 0.05	> 99
T132R/F189H	3.23 ± 0.05	> 99
T132R/F189Y	5.87 ± 0.12	> 99
T132 A/F189T	7.39 ± 0.07	> 99

[a] *Reaction conditions:* 40 °C, 100 mM Tris-HCl buffer (pH 7.5) containing 5% methanol, 20 mM *rac*-**1a**; reaction time, 5 min.
[b] Enantiomeric excess of product.

by choosing mutant T132R as a template. In total, 28 out of 372 clones (186 clones for each library) from the two libraries were selected because of their apparent higher activity and enantioselectivity towards *rac*-**1a**. After gene sequence analysis, six double mutants (T132R/F189C, T132R/F189S, T132R/F189T, T132R/F189H, T132R/F189Y, T132A/F189T) with superior activity (> 3 U/mg) and excellent enantioselectivity (ee_p > 99%) were obtained (Table 1). The double variant T132A/F189T (7.39 U/mg) showed the highest activity, which exhibited a 4.37-fold higher specific activity than that of the wild-type nitA (1.69 U/mg).

Kinetic Analysis of Nitrilase Variants

To elucidate the reason for the increase in the activity from a biochemical perspective, the steady-state kinetic parameters of wild-type nitA and its mutants were measured (Table 2). For the T132R variant, a 15% decrease in K_m combined with a 2.48-fold increase in k_{cat} contributed to a total 2.91-fold increase in k_{cat}/K_m. The enantioselectivity (E) for *rac*-**1a** was increased from 17.34 to 61.95, when compared to wild-type nitA. The K_m values of F189S and F189T were close to that of the wild-type nitA, indicating the similar substrate-binding affinity. The improved catalytic efficiency (k_{cat}/K_m) is mainly a result of the increase in their turnover frequencies. The mutant F189T has an excellent enantioselectivity (E > 200) towards *rac*-**1a**. When the variant site 189 was introduced while T132R as the template, the k_{cat} and catalytic efficiencies of double mutants (T132R/F189C, T132R/F189S, T132R/F189T, T132R/F189H, and T132R/F189Y) have not been improved in comparison with T132R or F189T. The combination of two best single mutants T132A and F189T (T132R/F189T) did not have a synergistic effect on improving enzymatic activity. However, the enantioselectivities of those variants have been improved greatly when compared to T132R. When the variant site 132 was introduced while F189T was the template, the double mutant T132A/F189T was found to have the highest V_{max} (8.27 μmol mg^{-1} min^{-1}) and stronger substrate-binding affinity. The catalytic efficiency (k_{cat}/K_m) of mutant T132A/F189T is 150.66 min^{-1} mM^{-1}, which is 7.26-fold higher than that of wild-type nitA. The T132A/F189T variant retained excellent enantioselectivity (E > 200).

Table 2. Comparison of the kinetic constants obtained for the wild-type and mutant enzymes.

Mutant (s)	Substrate	K_m [mM]	V_{max} [μmol mg^{-1} min^{-1}]	k_{cat} [min^{-1}]	k_{cat}/K_m [min^{-1} mM^{-1}]	E[a]
None (wild-type)	*rac*-**1a**	3.89	2.06	80.68	20.74	17.34
T132R	*rac*-**1a**	3.32	5.12	200.53	60.40	61.95
F189S	*rac*-**1a**	3.79	4.94	193.48	51.05	162.87
F189T	*rac*-**1a**	3.75	7.52	294.53	78.54	> 200
T132R/F189C	*rac*-**1a**	3.65	7.08	277.30	75.97	> 200
T132R/F189S	*rac*-**1a**	3.60	5.53	216.59	60.16	> 200
T132R/F189T	*rac*-**1a**	3.77	7.34	287.48	76.26	> 200
T132R/F189H	*rac*-**1a**	3.53	3.15	123.38	34.95	> 200
T132R/F189Y	*rac*-**1a**	3.41	4.73	185.26	54.33	> 200
T132A/F189T	*rac*-**1a**	2.15	8.27	323.91	150.66	> 200
None (wild-type)	*rac*-**1b**	5.71	1.18	46.22	8.10	5.70
None (wild-type)	*rac*-**1c**	6.23	2.54	99.48	15.97	5.21
None (wild-type)	*rac*-**1d**	1.89	8.06	315.68	167.03	150.12
T132A/F189T	*rac*-**1b**	2.89	0.29	11.36	3.92	5.62
T132A/F189T	*rac*-**1c**	1.76	0.03	1.18	0.67	5.41
T132A/F189T	*rac*-**1d**	4.33	2.37	92.83	21.44	134.67

[a] Enantioselectivity, which was calculated using the following formula[23] $E = \ln[1-c(1+ee_p)]/\ln[1-c(1-ee_p)]$, where c is conversion and ee_p is enantiomeric excess of product.

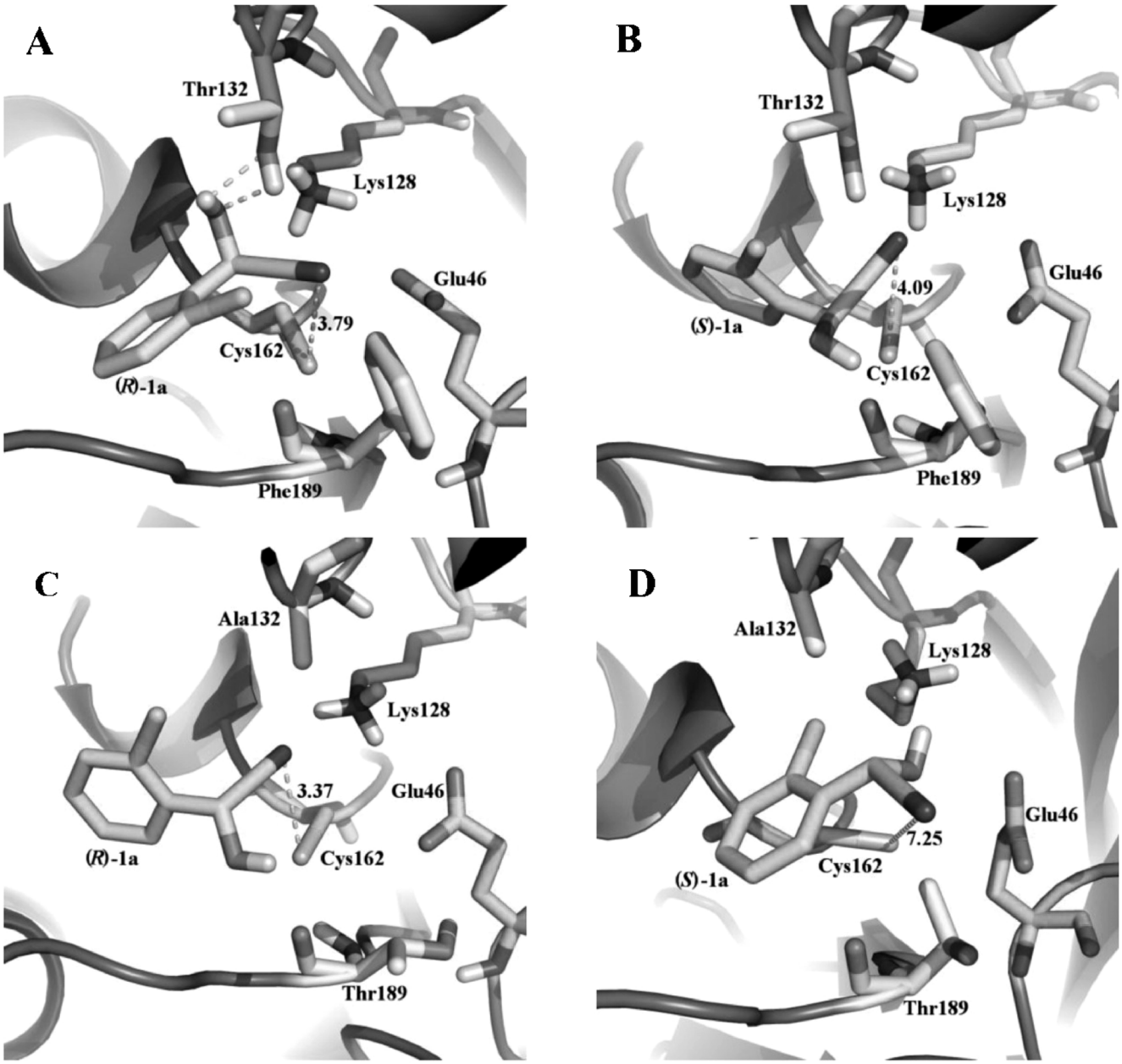

Figure 2. Molecular docking of (*R*)-**1a** and (*S*)-**1a** (dark grey sticks) into the active site of wild-type (**A**, **B**) and mutant T132A/F189T (**C**, **D**). The catalytic residues Glu46-Lys128-Cys162 and mutant sites (132, 189) were shown as medium grey sticks and light grey sticks, respectively. The dockings of substrates were performed using AutoDock 4.0. The figures were generated using PyMOL.

We also investigated the effect of the chloro-substituent position in the substrate on the catalytic performance and enantioselectivity of wild-type nitA and T132A/F189T variant. For wild-type nitA, the k_{cat} and catalytic efficiency towards various substrates with a chloro substituent in *ortho*-, *meta*-, or *para*-position in the phenyl ring decrease significantly because of the steric hindrance. Meanwhile, the enantioselectivity also decreased greatly. The substrate without the substituted group in the phenyl ring (*rac*-**1d**) is the most favorable substrate for the wild-type nitA. For mutant T132A/F189T, the highest activity and enantioselectivity were observed towards *ortho*-substituted substrate *rac*-**1a** and a general trend can be found that the activity and enantioselectivity decrease as the chloro substituent on the phenyl ring is shifted from the *ortho*-position to the *para*-position.

Characterization of nitA Wild-Type and T132A/F189T by Molecular Modeling

In order to illustrate the differences in activity and enantioselectivity between the wild-type nitA and the

best mutant T132A/F189T, we modeled the *R*- and *S*-enantiomers of *rac*-**1a** into the active site of wild-type and mutant nitA. According to the proposed nitrilase reaction mechanism,[22] the distance between the sulfur of the sulfhydryl group on the catalytic Cys162 and the cyano carbon in the substrate plays a crucial role in determining the nitrilase catalytic activity towards the substrate. For wild-type nitA, the distances between the sulfur of sulfhydryl group on the catalytic Cys162 with the cyano carbon in the substrate (*R*)-**1a** and (*S*)-**1a** were 3.79 and 4.09 Å, respectively (Figure 2A and B). The Cys162 could attack the cyano carbon in (*R*)-**1a** as well as in (*S*)-**1a** as a nucleophile, resulting in a poor enantioselectivity ($E=17.34$). In addition, there are two strong hydrogen bonds between the hydroxy in the substrate (*R*)-**1a** and Thr 132, which might hinder the release of product, leading to a low activity. For mutant T132A/F189T, the distance between the sulfur of the sulfhydryl group on the catalytic Cys162 and the cyano carbon in (*R*)-**1a** is 3.37 Å (Figure 2). The nucleophilic attack on this cyano carbon becomes easier by virtue of the proper orientation and distance. However, the distance for (*S*)-**1a** was 7.25 Å, which is too remote to initiate the nucleophilic attack for the sulfhydryl group (Figure 2D). So, the mutant T132A/F189T displayed high activity and enantioselectivity towards *rac*-**1a**. The result was in agreement with the analysis of kinetics parameters, which implied that the binding affinity of T132A/F189T to (*R*)-**1a** has been significantly improved. The increased activity for T132A/F189T might be caused by the increase in steric bulk introduced for (*R*)-**1a** but not for (*S*)-**1a** due to the short side chain in Ala132 and Thr189, resulting in a low steric hindrance towards a chloro substituent at the *ortho*-position. It benefits the substrate (*R*)-**1a** to enter the catalytically active center and change its orientation to be easily attacked by the sulfur of the sulfhydryl group in Cys162 with a shorter distance. Meanwhile, there is no strong hydrogen bond between the α-hydroxy of the substrate with Ala132. The product could be released easily, which facilitates the next substrate molecule to enter the catalytically active center. The similar situation was also observed for F189T and F189S. For T132R, although Arg132 in this single mutant has a long side chain, its side chain was towards the opposite of catalytic pocket and played the same role as Ala132. The mutant T132R enlarged the pocket and made it possible for Phe189 to be replaced with other residues (Cys, Ser, Thr, His and Tyr) with higher activity than wild-type nitA. All of the single mutants and double mutants at 132 and 189 obtained in this work showed higher activity and enantioselectivity towards *rac*-**1a** than wild-type nitA, implying that the sites 189 and 132 determine the activity and enantioselectivity. When substrates (*R*)-**1b–1d** and (*S*)-**1b–1d** were docked into the active site of mutant, the Cys162 could attack the cyano carbon in both *R*-isomer and *S*-isomer as a nucleophile (Supporting Information, Figure S2), resulting in the poorer enantioselectivity. Meanwhile, there are strong hydrogen bonds formed between the hydroxy in Thr189 and the α-hydroxy in (*R*)-**1b–1d**, which could hinder the release of product and decrease the activity.

Preparative Application of Mutant Nitrilase for the Synthesis of (*R*)-1a

The catalytic property of T132A/F189T was investigated to explore its potential as a candidate biocatalyst for the resolution of *rac*-**1a**. In comparison to isolated nitrilase, whole-cell biotransformation is more stable due to the presence of their natural environment inside the cells. We selected the whole cells of recombinant *E. coli* BL21(DE3) harboring plasmid pET-28b (+)-T132A/F189T as biocatalyst. The insolubility of nitrile substrates in the aqueous reaction mixture could lead to the mass-transfer problem, thereby decreasing the enzymatic reaction rate.

The aqueous-organic biphasic system can enhance the availability of insoluble nitrile substrate to the nitrilase active site, thereby increasing the catalytic efficiency.[12] The preselected aqueous-organic biphasic system, toluene-water (2:8, v/v) system, was used in the enantioselective hydrolysis of *rac*-**1a**. The various concentrations of substrate from 100 mM to 400 mM were used to evaluate the catalytic activity towards *rac*-**1a**. The whole cells of recombinant *E. coli* performed well from 100 mM to 300 mM, giving (*R*)-**2a** in $>90\%$ conversion and $>99\%$ ee_p. As the *rac*-**1a** concentration was increased to 400 mM, little (*R*)-**2a** was produced because the high concentration of nitrile was harmful to nitrilase. The enantioselective hydrolysis with 100 mM of (*R*)-**2a** exhibited the highest substrate conversion of up to 96.7% (Figure 3). In order to produce (*R*)-**2a** at higher substrate conversion, a fed-batch reaction mode was tried in the preselected toluene-water (2:8, v/v) system. The initial *rac*-**1a** concentration was set at 100 mM. When the substrate was exhausted in the first batch reaction, 100 mM of *rac*-**1a** were supplemented per 20 min for the fed-batch reaction. Pleasingly, the cumulative (*R*)-**2a** amount reached as high as 450 mM with 90% conversion and $>99\%$ ee_p within 3 h (Figure 4). The productivity was 671.76 $g L^{-1} d^{-1}$ without any loss of ee_p, which markedly exceeded the average productivity of industrial bioprocess (372 $g L^{-1} d^{-1}$).[24] After recrystallization in toluene, (*R*)-**2a** was obtained as a while solid in 87% isolated yield and $>99\%$ ee_p. Compared with the existing nitrilase aimed at producing (*R*)-**2a** (Table 3), the mutant T132A/F189T-mediated biocatalytic resolution gave higher substrate loading, enantio-

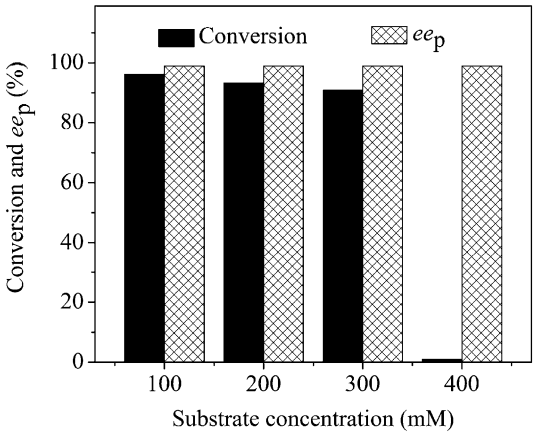

Figure 3. The effect of substrate concentration on conversion and ee_p. *Reaction conditions:* 100 mM Tris-HCl buffer (pH 7.5) containing 20% toluene, 0.3 g dry cells, 100–400 mM (final concentration) *rac*-**1a**, 40 °C.

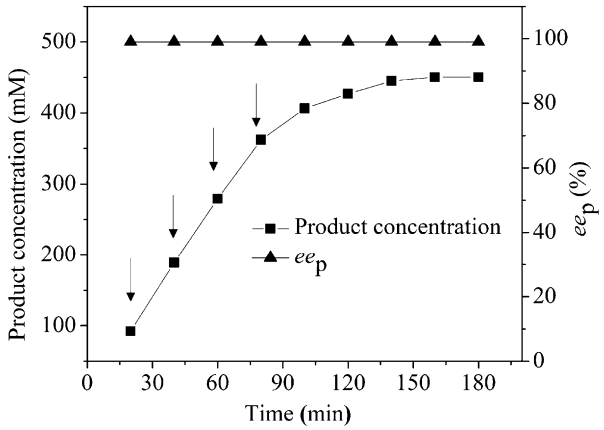

Figure 4. Regioselective hydrolysis of *rac*-**1a** for synthesizing (*R*)-**2a** with whole cells of recombinant *E. coli* BL21(DE3) harboring plasmid pET-28b(+)-T132A/F189T by fed-batch mode in biphasic system. *Reaction conditions:* 100 mM Tris-HCl buffer (pH 7.5) containing 20% toluene, 40 °C, 0.3 g dry cells, and 100 mM *rac*-**1a** was added per 20 min.

selectivity, and productivity, making it promising and competitive for practical application.

Conclusions

In summary, the activity and enantioselectivity of nitA towards *rac*-**1a** could be improved by a structure-based rational design approach. Several single mutants and double mutants with superior nitrilase activity (>3 U/mg) and enantioselectivity (>99% ee_p) have been identified based on molecular docking experiments, followed by the screening assay based on the hydrolytic activities towards substrate *rac*-**1a**. The key residues (132, 189) which determine the activity and enantioselectivity towards *ortho*-chloromandelonitrile were found. The best mutant T132A/F189T displays higher activity, productivity and enantioselectivity in the hydrolysis of *rac*-**1a** than all the reported nitrilases, which renders this variant to be a very suitable candidate for practical application in the kinetic resolution of *rac*-**1a** to (*R*)-**2a**, a key intermediate for the synthesis of anti-thrombotic agent (*S*)-clopidogrel, which is one of the best-selling drugs for heart attack and stroke treatment. Further studies, including engineering of nitrilases towards another 2-hydroxyarylacetonitriles to produce valuable chiral 2-hydroxyarylacetic acids based on this work, are in progress.

Experimental Section

Strains, Plasmids and Chemicals

The nitrilase gene (GeneBank: AY487562) with a length of 1014 bp was synthesized after condons optimization by software against *E. coli* as host according to the method as described previously.[15c] The restriction sites *Nco*I and *Xho*I were introduced at both ends. The ATG in *Nco*I acted as the initiation codon with an insertion of Gly at second residues. *E. coli* JM109 (Tiangen Biotech. Co. Ltd., Beijing, China) and plasmid pMD18-T (Takara, Dalian, China) were used for gene cloning experiments. The BL21 (DE3) (Novagen, USA) and pET-28b(+) (Novagen, USA) were applied for recombinant protein expression. (*R*)-**2a–2d** were purchased from J&K Chemical Co., Ltd. (Shanghai, China). All the other chemicals used were of analytical grade and commercially available.

Table 3. Comparison on enantioselective hydrolysis of *rac*-**1a** with the reported nitrilases.

Entry	Biocatalyst	Substrate loading [mM]	Conversion [%]	ee_p [%]	Productivity [$g L^{-1} d^{-1}$]	Ref.
1	Nitrilase 1	50	92	96	n.a.[a]	[9]
2	pHNIT45	10	100	99	268.70	[10]
3	*E. coli* JM109/pNLE	200	76.5	90.4	171.30	[11]
4	LaN	300	94.5	96	154.4	[12]
5	BCJ2315	494	84	97.6	232.32	[13]
6	T132A/F189T	500	90	>99	671.76	this work

[a] Not available.

Library Construction and Screening

The active site residues at positions 52, 132, 189 and 190 were selected to create saturation mutagenesis libraries. The corresponding forward and reverse primers (Supporting Information, Table S1) were designed by Primer X. The combinatorial saturation mutagenesis library at site 132 was constructed using mutant F189T as a template. The combinatorial saturation mutagenesis library at site 189 was constructed using mutant T132R as a template. The PCR products were digested with *Dpn* I to remove parent plasmid (2 h at 37 °C with 10 units of *Dpn* I), then the reaction mixtures were transformed into *E. coli* BL21(DE3) and plated on Luria-Bertani (LB) medium (Yeast extract, 5 $g L^{-1}$; Peptone, 10 $g L^{-1}$; NaCl, 10 $g L^{-1}$; pH 7.0) agar plates containing 50 $\mu g mL^{-1}$ kanamycin.

All clones containing several parent *E. coli* were grown in the respective wells in 96-well plates, in 2.2 mL growblock (Axygen) that contained 1.0 mL LB medium with 50 $\mu g mL^{-1}$ kanamycin. The plates were incubated at 37 °C and 200 rpm. When OD_{600} reached 0.5–0.6, 0.1 mM isopropyl-β-D-1-thiogalactopyranoside (IPTG) was added. Then the cultivation was continued at 28 °C for 10 h. Cells were harvested by centrifugation (4 °C, 3,000 × *g*, 30 min). The cell pellets were then resuspended in Bugbuster solution (0.5 mL) and the plates were incubated at room temperature with agitation for 30 min. The hydrolysis reactions (1 mL) containing Tris-HCl buffer (100 mM, pH 7.5), 20 mM *rac*-**1a**, 5% methanol and 100 μL of the cell free extracts were carried out at 40 °C by using a Thermomixer Compact (Eppendorf, Germany) for 5 min, to which were added 10 μL HCl (6.0 M). The activity and enantioselectivity of nitrilase were detected by chiral HPLC as described below.

Expression and Purification of Nitrilase Variants

Recombinant *E. coli* harboring the plasmid pET-28b(+) containing the wild-type nitA or a mutant nitA gene with a histidine tag at the carboxyl terminus was grown in LB liquid medium containing 50 $\mu g mL^{-1}$ kanamycin at 150 rpm and 37 °C. Nitrilase expression was induced by adding IPTG to a final concentration of 0.1 mM when the optical density reached 0.5–0.6 and then continuously incubated at 28 °C for 10 h. After centrifugation at 9,000 rpm under 4 °C for 20 min, the cells were harvested and preserved for further experiments.

These mutants and wild-type nitA were produced in the cytoplasm of *E. coli* BL21(DE3) and purified to >90% homogeneity using an Ni-based immobilized metal affinity chromatography procedure.[15b] The evaluations of activity and ee_p were performed by the standard assay with the purified nitrilases.

Analytical Methods

The concentration and optical purity of hydrolysis products of *rac*-**1a** and *rac*-**1d** were determined by chiral HPLC equipped with a reverse phase chiral column (Astec Chirobiotic™ R 250 × 4.6 mm, Sigma, USA), and A_{215} was measured. The mobile phase contained 0.5% AcOH-CH_3CN (12:88, v/v) with a flow rate of 1.0 $mL min^{-1}$. The temperature of elution was 30 °C.

The concentrations of hydrolysis products of *rac*-**1b** and *rac*-**1c** were analyzed by HPLC equipped with a Hypersil ODS (24.6 mm × 250 mm, 5.0 μm) column and A_{215} was measured. The mobile phase was composed of $NH_4H_2PO_4$ (50 mM) and water at a ratio of 35:65 (v/v) with a flow rate of 1.0 $mL min^{-1}$. The temperature of elution was set at 30 °C. For determining the optical purity of the hydrolysis products of *rac*-**1b** and *rac*-**1c**, samples were esterified using boron trifluoride in methanol and subjected to chiral HPLC using a Chiralcel OD column (250 mm × 4.60 mm, 5 μm; Daicel Chemical Industries, Japan) and A_{228} was measured. The mobile phase contained *n*-hexane, isopropyl alcohol and trifluoroacetic acid (90:10:0.1, v/v) with a flow rate of 0.8 $mL min^{-1}$. The temperature of elution was set at 30 °C.

For determining the enzyme activity, the reactions were performed at 40 °C for 5 min by using a Thermomixer Compact (Eppendorf, Germany). The reaction mixture contained (1.0 mL) Tris-HCl buffer (100 mM, pH 7.5), 20 mM substrate, 5% methanol and an appropriate amount of pure enzyme. The reactions were stopped by adding 10 μL HCl (6.0 M). The product concentrations were detected by HPLC. One unit of the enzyme activity (U) was defined as the amounts of enzyme that produce 1.0 μmol products per minute under the standard assay conditions.

Determinations of Kinetics Parameters

The kinetic analysis of wild-type and mutant nitA were carried out in Tris-HCl buffer (pH 7.5, 100 mM) at 40 °C with purified nitrilases. The final substrate concentration was 0.8–3.0 mM and the reactions were stopped by the addition of 10 μL HCl (6.0 M). The product concentration of was detected. The values of K_m and V_{max} were obtained by the Lineweaver–Burk double-reciprocal method. The value of k_{cat} was calculated by using the equation $k_{cat} = V_{max}/[E]$.

Molecular Homology Modeling and Docking

The three-dimensional homology models of nitrilases were generated by the program Modeller 9.12 using crystal structures of protein PH0642 (PDB accession code 1J31, resolution 1.6 Å) as template. Docking experiments were performed using the program AutoDock 4.0, and the images were created using PyMOL. The best quality model generated by Modeller 9.12 has the highest GA341 score and the lowest DOPE score. The model was evaluated by Procheck and Profile-3D (http://www.ebi.ac.uk/thornton-srv/databases/pdbsum/Generate.html). The nitA showed 25% sequence identity with the protein from *P. horikoshii*. The catalytic triad (Glu46-Cys162-Lys128) of nitA and PH0642 of the same nitrilase superfamily were completely conserved. Moreover, the homology model of nitA has a four-layer α-β-β-α sandwich fold which is similar to other nitrilase superfamily members (Supporting Information, Figure S3). Procheck and profile-3D were used to evaluate the modeled structure. The best quality model of nitA was shown in the Ramachandran plot, where 82.4% residues were located in the most favored regions, 13.1% in the additional allowed regions, and 2.4% in the generously allowed regions. Only 2.1% were located in disallowed regions. Most of the residues in disallowed regions were located at the end of the carbon terminal and far away from the catalytic center. The results from Profile-3D showed that the overall compatibili-

ty score for this model was 107.8 in the scale of the expected value 69.69–154.87. All these data indicated that the model of nitA was reliable. Structure-based sequence alignment was performed using the program Clustal X and the picture of the sequence alignment was made using the program ESPRIPT.

Whole-Cell Biocatalysis of *rac*-1a in a Biphasic System

In a biphasic system, there were 100 mL of the reaction mixture in a 250-mL conical flask, consisting of 100 mM Tris-HCl buffer (pH 7.5), 0.3 g dry cells, and 20% toluene. For batch reactions, 100, 200, 300 and 400 mM *rac*-**1a** were added to start the reactions, respectively. The reaction mixtures were stirred by magnetic agitation with a water jacket thermostatted at 40 °C. The pH was automatically adjusted to 7.5 by titrating 1.0 M ammonia. For the fed-batch reaction, the initial *rac*-**1a** concentration was set at 100 mM. Subsequent feedings were carried out with 100 mM *rac*-**1a** at an interval of 20 min. The total amount of *rac*-**1a** was 500 mM. Samples (500 μL) were withdrawn at required time intervals and determined by chiral HPLC. The product was (*R*)-**2a** and no amides were formed. When the substrate was almost exhausted, the cells were removed by centrifugation. The aqueous phase was acidified to pH 1.0 with 2 M HCl and extracted twice with equal volumes of ethyl acetate. The organic phase was dried by anhydrous sodium sulfate and then evaporated under vacuum. The resulting solid was recrystallized using toluene as solvent to obtained (*R*)-**2a**; yield: 7.3 g (87.0); >99% ee_p; $[\alpha]_D^{20}$: −151.6 (*c* 0.5, ethanol). Lit.[25] $[\alpha]_D^{25}$: −154.5 (*c* 0.52, ethanol). ^{1}H NMR (500 MHz, D_2O): δ = 7.38–7.33 (m, 1H), 7.30 (ddd, *J* = 10.7, 6.0, 3.3 Hz, 1H), 7.27–7.19 (m, 2H), 5.51 (s, 1H); ^{13}C NMR (126 MHz, D_2O): δ = 175.65 (s), 135.52 (s), 133.06 (s), 130.60 (s), 130.07 (s), 129.44 (s), 127.76 (s), 70.43 (s); HR-MS (ESI): *m/z* = 184.9996, calcd. for $C_8H_6ClO_3$ $[M]^-$: 185; IR (KBr): ν = 3379, 3199, 2927, 1750, 1694, 1477, 1444, 1423, 1264, 1217, 1191, 1128, 1072, 1035, 930, 821, 748, 688 cm^{-1}.

Acknowledgements

This work was supported by the National Natural Science Foundation of China (No. 31170761) and the 863 Program (No. 2011AA02A210).

References

[1] H. Gröger, *Adv. Synth. Catal.* **2001**, *343*, 547–558.
[2] a) L. M. van Langen, F. van Rantwijk, R. A. Sheldon, *Org. Process Res. Dev.* **2003**, *7*, 828–831; b) T. Ema, S. Ide, N. Okita, T. Sakai, *Adv. Synth. Catal.* **2008**, *350*, 2039–2044.
[3] C. C. Gruber, I. Lavandera, K. Faber, W. Kroutil, *Adv. Synth. Catal.* **2006**, *348*, 1789–1805.
[4] J. Balint, M. Csatarine Nagy, Z. Dombrady, E. Fogassy, A. Gajari, C. Suba, *PCT Int. Appl.* WO 0300636, **2003**.
[5] B.-D. Ma, X. Kong, H.-L. Yu, Z.-J. Zhang, S. Dou, Y.-P. Xu, Y. Ni, J.-H. Xu, *ACS Catal.* **2014**, *4*, 1026–1031.
[6] S. Rustler, A. Müller, V. Windeisen, A. Chmura, B. C. M. Fernandes, C. Kiziak, A. Stolz, *Enzyme Microb. Technol.* **2007**, *40*, 598–606.
[7] a) C. Vergne-Vaxelaire, F. Bordier, A. Fossey, M. Besnard-Gonnet, A. Debard, A. Mariage, V. Pellouin, A. Perret, J.-L. Petit, M. Stam, M. Salanoubat, J. Weissenbach, V. De Berardinis, A. Zaparucha, *Adv. Synth. Catal.* **2013**, *355*, 1763–1779; b) S. J. Wu, A. J. Fogiel, K. L. Petrillo, E. C. Hann, L. J. Mersinger, R. DiCosimo, D. P. O'Keefe, A. Ben-Bassat, M. S. Payne, *Biotechnol. Bioeng.* **2007**, *97*, 689–693.
[8] S. Bergeron, D. A. Chaplin, J. H. Edwards, B. S. W. Ellis, C. L. Hill, K. Holt-Tiffin, J. R. Knight, T. Mahoney, A. P. Osborne, G. Ruecroft, *Org. Process Res. Dev.* **2006**, *10*, 661–665.
[9] G. DeSantis, Z. Zhu, W. Greenberg, K. Wong, J. Chaplin, S. Hanson, B. Farwell, L. Nicholson, C. Rand, D. Weiner, D. Robertson, M. Burk, *J. Am. Chem. Soc.* **2002**, *124*, 9024–9025.
[10] U. Schreiner, B. Hecher, S. Obrowsky, K. Waich, N. Klempier, G. Steinkellner, K. Gruber, J. D. Rozzell, A. Glieder, M. Winkler, *Enzyme Microb. Technol.* **2010**, *47*, 140–146.
[11] Z. J. Zhang, J. A. Pan, J. F. Liu, J. H. Xu, Y. C. He, Y. Y. Liu, *J. Biotechnol.* **2011**, *152*, 24–29.
[12] C. S. Zhang, Z. J. Zhang, C. X. Li, H. L. Yu, G. W. Zheng, J. H. Xu, *Appl. Microbiol. Biotechnol.* **2012**, *95*, 91–99.
[13] H. L. Wang, H. H. Sun, W. Y. Gao, D. Z. Wei, *Org. Process Res. Dev.* **2014**, *18*, 767–773.
[14] a) H. P. Dong, Z. Q. Liu, Y. G. Zheng, Y. C. Shen, *Appl. Microbiol. Biotechnol.* **2010**, *87*, 1335–1345; b) Y. G. Zheng, J. Chen, Z. Q. Liu, M. H. Wu, L. Y. Xing, Y. C. Shen, *Appl. Microbiol. Biotechnol.* **2008**, *77*, 985–993; c) Q. Zhu, A. Fan, Y. S. Wang, X. Q. Zhu, Z. Wang, M. H. Wu, Y. G. Zheng, *Appl. Environ. Microbiol.* **2007**, *73*, 6053–6057.
[15] a) Z. Q. Liu, P. J. Baker, F. Cheng, Y. P. Xue, Y. G. Zheng, Y. C. Shen, *Plos One* **2013**, *8*(6), e67197; b) Z. Q. Liu, L. Z. Dong, F. Cheng, Y. P. Xue, Y. S. Wang, J. N. Ding, Y. G. Zheng, Y. C. Shen, *J. Agric. Food Chem.* **2011**, *59*, 11560–11570; c) L. Q. Jin, Z. T. Li, Z. Q. Liu, Y. G. Zheng, Y. C. Shen, *J. Ind. Microbiol. Biotechnol.* **2014**, *41*, 1479–1486.
[16] Z. Q. Liu, X. H. Zhang, Y. P. Xue, M. Xu, Y. G. Zheng, *J. Agric. Food Chem.* **2014**, *62*, 4685–4694.
[17] D. M. Zhu, Y. Yang, S. Majkowicz, T. H. Y. Pan, K. Kantardjieff, L. Hua, *Org. Lett.* **2008**, *10*, 525–528.
[18] a) J. S. Gong, Z. M. Lu, H. Li, Z. M. Zhou, J. S. Shi, Z. H. Xu, *Appl. Microbiol. Biotechnol.* **2013**, *97*, 6603–6611; b) L. Martinkova, V. Vejvoda, V. Kren, *J. Biotechnol.* **2008**, *133*, 318–326.
[19] D. E. Robertson, J. A. Chaplin, G. DeSantis, M. Podar, M. Madden, E. Chi, T. Richardson, A. Milan, M. Miller, D. P. Weiner, K. Wong, J. McQuaid, B. Farwell, L. A. Preston, X. Tan, M. A. Snead, M. Keller, E. Mathur, P. L. Kretz, M. J. Burk, J. M. Short, *Appl. Environ. Microbiol.* **2004**, *70*, 2429–2436.
[20] a) J. E. Raczynska, C. E. Vorgias, G. Antranikian, W. Rypniewski, *J. Struct. Biol.* **2011**, *173*, 294–302; b) N. Sakai, Y. Tajika, M. Yao, N. Watanabe, I. Tanaka, *Proteins Struct. Funct. Bioinf.* **2004**, *57*, 869–873.

[21] a) T. Koudelakova, R. Chaloupkova, J. Brezovsky, Z. Prokop, E. Sebestova, M. Hesseler, M. Khabiri, M. Plevaka, D. Kulik, I. K. Smatanova, P. Rezacova, R. Ettrich, U. T. Bornscheuer, J. Damborsky, *Angew. Chem.* **2013**, *125*, 2013–2017; *Angew. Chem. Int. Ed.* **2013**, *52*, 1959–1963; b) U. T. Bornscheuer, G. W. Huisman, R. J. Kazlauskas, S. Lutz, J. C. Moore, K. Robins, *Nature* **2012**, *485*, 185–194; c) L. F. Godinho, C. R. Reis, R. van Merkerk, G. J. Poelarends, W. J. Quax, *Adv. Synth. Catal.* **2012**, *354*, 3009–3015.

[22] a) L. Martinkova, V. Kren, *Curr. Opin. Chem. Biol.* **2010**, *14*, 130–137; b) H. C. Pace, S. C. Hodawadekar, A. Draganescu, J. Huang, P. Bieganowski, Y. Pekarsky, C. M. Croce, C. Brenner, *Curr. Biol.* **2000**, *10*, 907–917.

[23] C. S. Chen, Y. Fujimoto, G. Girdaukas, C. J. Sih, *J. Am. Chem. Soc.* **1982**, *104*, 7294–7299.

[24] A. S. Bommarius, B. R. Riebel-Bommarius, *Biocatalysis: fundamentals and applications*, Wiley-VCH, Weinheim, **2007**.

[25] N. Kurono, T. Yoshikawa, M. Yamasaki, T. Ohkuma, *Org. Lett.* **2011**, *13*, 1254–1257.

